Low-temperature synthesis of large-area graphene-based carbon films on Ni

Lu, Liqiang; De Hosson, J.T.M.; Pei, Yutao

Published in:
Materials & design

DOI:
10.1016/j.matdes.2018.02.034

Publication date:
2018

Low-temperature synthesis of large-area graphene-based carbon films on Ni

Liqiang Lu[1], Jeff T.M. De Hosson[2], Yutao Pei[1*]

[1] *Department of Advanced Production Engineering, Engineering and Technology Institute Groningen, Faculty of Science and Engineering, University of Groningen, Nijenborgh 4, 9747 AG Groningen, The Netherlands*

[2] *Department of Applied Physics, Zernike Institute for Advanced Materials, Faculty of Science and Engineering, University of Groningen, Nijenborgh 4, 9747AG Groningen, The Netherlands*

Abstract

In this work, large-area graphene-based carbon films were synthesized through a fast and low-temperature method. The processing route is illustrated on a free surface of Ni catalyst film by vacuum thermal processing of amorphous carbon. Key in the novel approach is that the synthesis is done at low temperatures, i.e. below 350 °C, and within a time as short as one minute. The nucleation and growth of graphene on the free surface of nickel and along the interface between Ni film and SiO_2 substrate are investigated by using a thin film Ni-C-Ni sandwiched structure on a SiO_2/Si substrate. Raman spectroscopy demonstrates that the graphene-based carbon films consist of graphitic carbon rich of defects. HR-TEM observations reveal that the graphene-based carbon film grown on the top free surface is composed of thin multilayer graphene segments (3-6 atomic layers) and thick multilayer graphene segments (more than atomic 10 layers), covering the entire surface of Ni film over a large area. Growth parameters such as growth time, growth temperature and carbon/Ni ratio are reported in detail for a control of graphene growth kinetics. The results point at several attractive strategies for the facile synthesis of graphene-based carbon films for industrial applications.

Key words: graphene film, growth behavior, low temperature, nickel, microscopy

* Corresponding author. E-mail: y.pei@rug.nl

1. Introduction

It goes without saying that graphene became an astonishing functional material in various fields of fundamental research and applications, e.g. electronics, energy conversion and storage, biological engineering, catalysis, environment protection, water purification etc. [1-7]. The synthesis of graphene films is vital for up-scaling in industrial applications. Chemical vapor deposition (CVD) made a considerable impact in large-area and large-scale graphene production based on sacrifices of catalyst (transition metals, ceramics, etc.) [8 , 9]. Unfortunately, CVD growth of graphene needs high temperature, i.e. ~1000 °C [8, 10], and also other thermal synthesis methods for producing graphene are executed at high temperatures [11,12]. The high processing temperature induces several critical issues, such as a limiting choice of substrates, expensive equipment, and it also requires a rather complex transfer process. Progress in exploring low temperature growth of graphene has been achieved through different strategies, for instance using liquid or solid carbon precursors, design of alloy catalysts, Sn catalyst, (microwave) plasma-enhanced CVD, and implanting carbon in metallic catalysts, etc. [13-20] and non-metallic substrates [22,23]. As a result low temperature growth of graphene has been broadly studied in many different fields, e.g. electrocatalysts, transparent conductive films (TCFs), anti-corrosion, biological coatings, etc. [14,16,18,19,22,23].

Although significant progress has been made in the field of low temperature growth of graphene by sacrificing metal catalysts, the growth mechanism and resulting microstructures are still not fully understood. The low-temperature growth mechanism of graphene cannot be simply explained by normal CVD processes. The growth mechanism of graphene on Ni by CVD has been elucidated as the rearrangement of the dissolved carbon atoms on nickel (111) from bulk nickel, driven by the different soluble capacities at different temperatures [24]. But for low temperature growth of graphene on nickel, many conditions have been altered, such as unfavorable decomposition temperature of hydrocarbon gases and the interaction between Ni and carbon, etc. Therefore the growth kinetics of graphene at lower temperatures is rather different [25,26]. Previous research concentrated on the use of amorphous carbon as feedstocks for graphene growth [27 - 32]. However, the graphene growth was performed at high temperatures (> 650 °C). No publication has reported the conversion of amorphous carbon to graphene on Ni surfaces at such a low temperature. As far as the mechanism is concerned there are also major differences. At high temperatures, the temperature and cooling rate significantly influence the growth of graphene on Ni as carbon segregation is mainly driven by the decrease of carbon solubility in Ni during cooling [8,11,27]. But at low temperatures, the solubility is

very low and is not affected. The diffusion and segregation processes of carbon differ from those at high temperatures and rely on the concentration gradients. Even in recent work reporting conversion of amorphous carbon to graphene at 250 °C by using tin as catalyst [21], only discontinuous graphene flakes were formed. In particular, Weatherup et al. reported that graphene with domain sizes of > 220 μm² could grow on polycrystalline Ni-Au catalyst films at 450-600 °C, indicating the possibility of large-area graphene growth [17]. It could be attributed to the growth crossing grain-boundaries which still needs experimental validations. However, for the majority of substrate materials such as polymers, glasses and even metals the processing temperature above 450 °C is still rather high.

Here we concentrate on the synthesis of large-area graphene-based carbon films through a fast and low-temperature method. To the best of our knowledge, there is no research reported on the thermal conversion of amorphous carbon to graphene on the free surface of Ni film and the interface of Ni/substrates at near-room temperatures (below 350 °C). The nucleation and growth behavior of graphene on the Ni free surface at near-room temperatures, and environmental influencing factors are still unknown. Therefore the objective is to focus on the graphene formation on free surface of Ni catalyst by diffusion and conversion of amorphous carbon under vacuum thermal processing (VTP) at low temperature of 350 °C. In particular, by using a sandwich Ni-C-Ni film deposited on SiO_2/Si substrate, we have investigated the nucleation and growth of graphene on a free surface of nickel film and at the interface of Ni/SiO_2. Growth parameters such as growth time, growth temperatures, carbon/Ni ratios and resultant microstructures are also examined for control of the growth kinetics.

2. Experimental

2.1 Deposition of multilayer Ni-C-Ni diffusion couples

Magnetron sputtering deposition was used for the preparation of the Ni-C-Ni films. Nanocrystalline Ni (nc-Ni) films were deposited using Ni plate target (99.95% purity). The initial pressure of the deposition chamber before sputtering was 5×10^{-6} mbar and the deposition pressure of argon was 5×10^{-3} mbar. For the deposition of Ni-C-Ni multilayer diffusion couples, nc-Ni film of about 100 nm thickness was deposited as the first layer on SiO_2 (300 nm thick)/Si substrates (ø100 mm); next, an amorphous carbon film was deposited on Ni film as the intermediate layer in the middle by using graphite targets (99.99% purity), and finally nc-Ni

film ~100 nm thick was deposited as the top layer. The thickness of the amorphous carbon intermediate layer was changed in the range between 10 nm and 100 nm.

2.2 Carbon diffusion and graphene growth

The as-deposited samples were transferred to a high vacuum chamber (< 10^{-6} mbar) and subsequently vacuum thermal processing was carried out at various temperatures from room temperature to 350 °C for different durations, from 1 min to 96 hrs, respectively. The heating rate was 100 °C/s. The cooling rate after annealing was in the range of 6-12 °C/min. In the following the graphene film grown on the free surface of Ni film is named free surface graphene and the one formed along the Ni/SiO_2 interface is called interface graphene.

Preparation of samples for TEM observation of graphene formation at low temperature was as follows: nanocrystalline Ni film with a thickness of ~20 nm was deposited onto a TEM C/Cu grid (purchased from Agar Scientific, 400 meshes, with carbon film). The carbon film on Cu grid could provide carbon atoms for graphene formation. The nc-Ni coated C/Cu grids were put into an ultrahigh vacuum chamber (< 10^{-6} mbar) for vacuum thermal processing at 350 °C for 12 hrs. After cooling down at a cooling rate of 6-8 °C/min, the specimens were studied through transmission electron microscopy (TEM).

2.3 Characterization

The microstructure of the Ni thin film and that of the grown graphene-based carbon films were scrutinized by using atomic force microscopy (AFM, Digital Instruments NanoScope IIIa), scanning electron microscopy (SEM, Philips FEG-XL30s and Hitachi SU8230 equipped with a top detector filtering system to provide enhanced electron detection specificity and an upper E×B detector with SE/BSE signal mixing function), X-ray diffraction (Bruker D8 Advance diffractometer equipped with a Cu Kα source (λ=0.15406 nm) and high resolution transmission electron microscopy (HR-TEM, JEOL JEM-2010F operated at 200 kV). The SEM observations were performed using an accelerating voltage from 0.5 to 20 kV. Fine contrast differentiation is achieved by selectivity filtering inelastic scattering electrons and directly detecting specific energy-back-scattered electrons on Hitachi SU8230. Free surface graphene was also transferred by using poly(methyl methacrylate) (PMMA) and etching away the nc-Ni film by 1 M $FeCl_3$, and keeping the bottom interface graphene on the SiO_2/Si substrates. The interface graphene was further transferred using PMMA and etching away the SiO_2 by HF (15%). The transferred free surface graphene and interface graphene were put

separately onto Cu grids for TEM characterization. Raman spectrum analyses were performed using 532 nm laser excitation.

3. Results and discussion

3.1 Synthesis of graphene-based carbon film on Ni free surface and Ni/SiO_2 interface

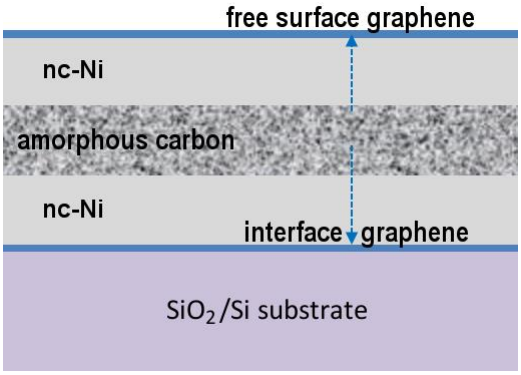

Fig. 1 Schematic illustration of the designed Ni-C-Ni sandwich film and graphene formation on the free surface of Ni film and at the interface of Ni/SiO_2 via vacuum thermal process (VTP). The thickness of nc-Ni layers was 100 nm, and the thickness of the amorphous carbon intermediate layer was varied between 10 and 100 nm.

Graphene can nucleate at the interface between Ni film and SiO_2/Si substrates and grows at room temperature [28]. However, it is unknown whether large-area graphene can form on a free surface of a nc-Ni film at such a low temperature, i.e. below 350 °C and whether a difference in graphene quality exists between free surface grown graphene and interface-induced graphene. Fig. 1 schematically illustrates the architecture of the triple Ni-C-Ni thin film, which was designed for simultaneous growth of graphene on Ni free surface and along the Ni/SiO_2 interface. The intermediate amorphous carbon film serves as a reservoir of carbon, providing carbon atoms for graphene growth. During low temperature vacuum thermal processing, carbon atoms diffuse through nc-Ni films and reach the surface of Ni and the interface of Ni/SiO_2, where they precipitate. Contrary to the case of graphite paste as carbon resource [28], sputter deposited amorphous carbon facilitates sp^2 carbon bond breaking. The quality of the Ni film deposited on the surface of the Ni-C-Ni sandwich structured film is studied by using AFM, SEM, and XRD. It was confirmed that nc-Ni films of good uniformity were deposited by the magnetron sputtering technique. The nc-Ni films with a grain size less than 20 nm were examined with XRD and SEM (see Supplementary Fig. S1). The surface roughness of the top nc-Ni film was about 0.1 nm (RMS roughness, see Supplementary Fig.

S2). For investigating the influence of the carbon reservoir on the growth of graphene carbon films with various thicknesses from 10 nm to 100 nm were deposited.

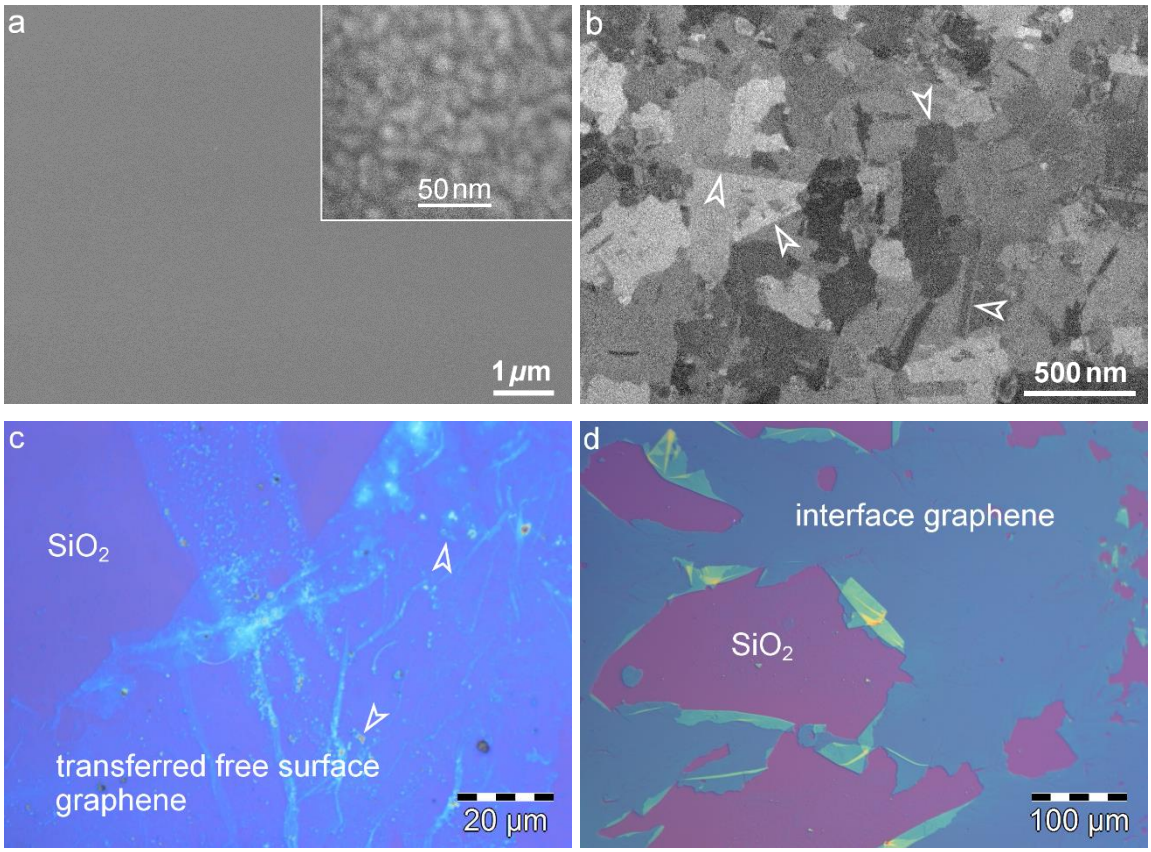

Fig. 2 SEM images showing the surface structure of Ni-C-Ni sandwich film before (a) and after (b) vacuum thermal processing at 350 °C for 12 h, with the inset of (a) at high magnification revealing a grainy surface morphology of the top Ni film before treatment, the white arrows in (b) point out the boundary of micron-sized multilayer graphene segments; Optical images of transferred free surface graphene-based carbon film from the Ni surface (c) and the remaining interface graphene-based carbon film on SiO_2 substrates after etching away Ni (d), the arrows in (c) show multilayer graphene fragments.

Figs. 2a and 2b display the surface of Ni-C-Ni sandwich film before and after vacuum thermal processing at 350 °C for 12 hrs. Before annealing a smooth and clean Ni surface with a grainy surface morphology was observed (see also the SEM micrograph in Fig. S1a and AFM image of Fig. S2 in the Supplementary). After vacuum thermal processing at 350 °C for 12 hrs, a continuous graphene-based carbon film emerged and covered the entire Ni surface. No evidence of any Ni carbide phase was found by XRD (not shown). As can be seen in Fig. 2b, the free surface graphene-based carbon film consists of micrometer graphene segments, which appear at different gray scales, indicating the formation of graphene segments of different thicknesses. The difference in graphene layer thickness induces a difference of surface potential

which affects the signal intensity of secondary electrons (SE) from the Ni film underneath [33]. These segments have special geometrical characteristics with sharp edges (marked by the white arrows). In contrast, a group of pure nanocrystalline Ni (nc-Ni) film without carbon source was exactly VTP treated at 350 °C for 1 h. The surface of such treated pure nc-Ni film (see Fig. S3) did not show the same profiles as observed in Fig. 2b. It demonstrates that the profiles shown in Fig. 2b are graphene segments, rather than possible texture and grain growth of nc-Ni film by thermal treatment. Fig. 2c and 2d show the optical images of the free surface graphene-based carbon film transferred from the Ni surface and the interface graphene-based carbon film left on SiO_2 substrates after removal of the Ni-C-Ni coatings. EDS was used to detect possible residuals on the transferred free surface film and leftover interface film. Ni and Fe remnants were not detected. Apparently, the interface graphene-based carbon film looks a bit thicker than the surface graphene-based carbon film due to the lower transparency. Wrinkles were formed but did not break during the transferring process, demonstrating the flexibility and good strength of 2D graphene. It should be mentioned that both of the free surface graphene-based carbon film and interface graphene-based carbon film are composed of graphene segments, which closely connect and become continuous films. The size of individual graphene segments, up to several microns, is much larger than the size of Ni grains, suggesting a growth mechanism thereby crossing Ni grain boundary even at such a low temperature.

Raman spectroscopy was carried out to understand the structural information of graphene-based carbon films. Fig. 3a and 3c show the Raman spectrum of free surface graphene and interface graphene, respectively. The free surface graphene-based carbon film as well as the interface graphene-based carbon film exhibit D band, G band, and a weak 2D band. For the free surface film, the D band, which is triggered by the defects, appears at 1354 cm^{-1}. The G band appeared at 1575 cm^{-1} is the characteristic of graphite, corresponding to the high-frequency E_{2g} phonon at Γ. The 2D band appeared at 2680 cm^{-1} is a multiple step mode of carbon [34]. The ratio of I_D/I_G is 1.80 from Fig. 3b for the free surface graphene, indicating that the as-synthesized film contains high content of defects. Compared with the Raman features of amorphous carbon, which has a G peak at ~1500 cm^{-1} and a I_D/I_G value around 0, the free surface graphene-based carbon film is different from amorphous carbon, and seem to have similar Raman features with nanocrystalline graphite [35]. For the interface graphene, the D band appears at 1355 cm^{-1}, and G band at 1597 cm^{-1}, respectively. A higher I_D/I_G value of 2.8 suggests that the interface graphene film has a higher content of defects and a lower graphitization than the free surface graphene. The larger full width at half-maximum (FWHM)

ranges of peaks (as seen in Table S1) for the interface graphene film suggest closer distances between defects (L_D) [36]. In addition, from the deconvolution of Raman spectra of the free surface graphene film and the interface graphene film shown in Fig. 3b and 3d, both have D* band located at Raman shift between 1150 and 1200 cm^{-1}, D" band in the range between 1500 and 1550 cm^{-1}, and D' band at ~1622 cm^{-1} [37]. According to the previous studies, all the D*, D' and D" related to the disordered graphitic structure and amorphous phases [37, 38, 39, 40].

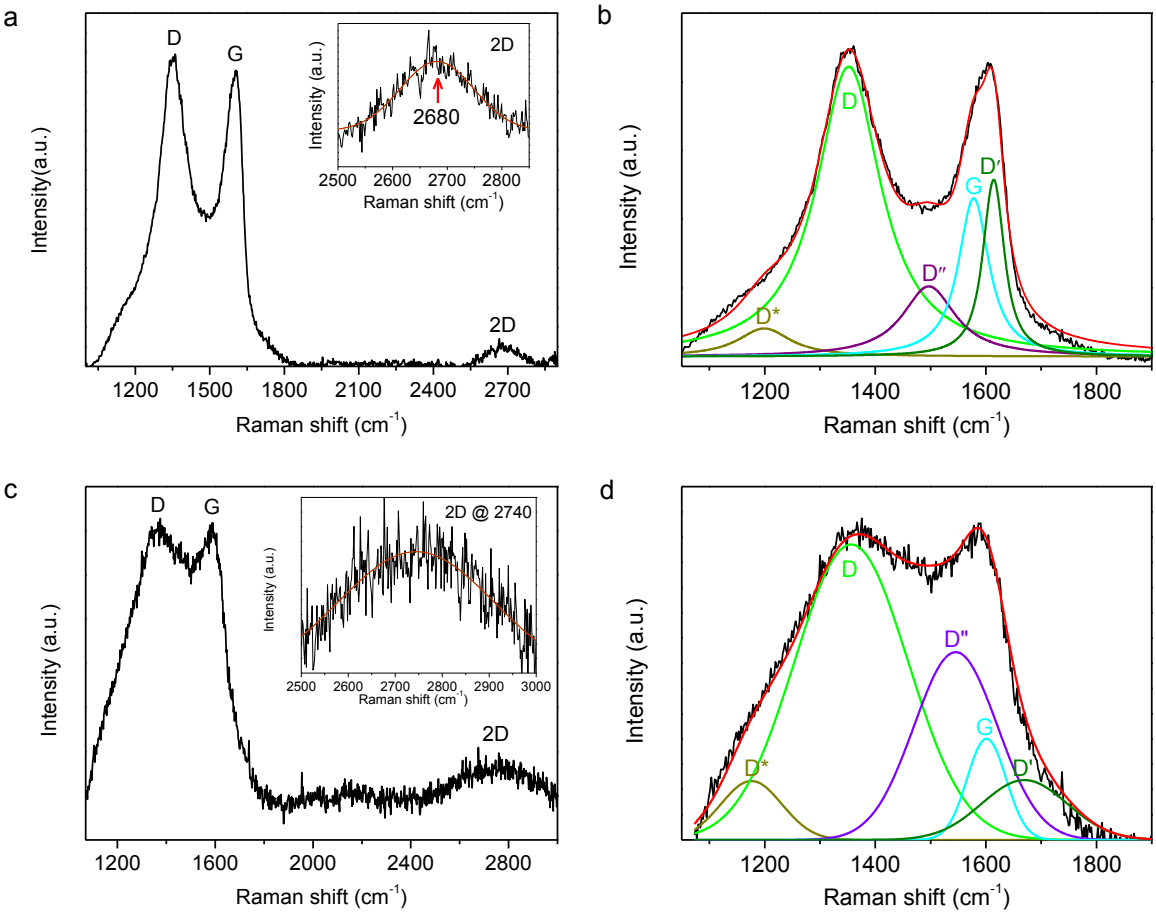

Fig. 3 Raman spectra of graphene-based carbon films VTP processed at 350 °C for 12 h: (a) free surface graphene-based carbon film with an insert of the fitted 2D band; (b) deconvolution of Raman spectrum of (a) from 1000-1900 cm^{-1}; (c) interface graphene-based carbon film with an inset of the fitted 2D band; (d) deconvolution of Raman spectrum of (c) from 1000-1900 cm^{-1}.

The intensity of D" band decreases with the increase of the crystallinity. The enhanced D" band and bigger FWHM range of D" peak for the interface graphene imply the lower graphitization and smaller L_D compared with the free surface graphene. The reason is still not fully resolved. It should be realized that, both the free surface graphene film and the interface graphene film possess a high concentration of defects, causing the broadened peaks and low intensities [41]. These defects are formed mainly due to the low-temperature growth process. Another issue is

that the films may contain a little amount of amorphous carbon attached on the graphene surface, as carbon atoms keep diffusing particularly along the Ni grain boundaries during the cooling processes.

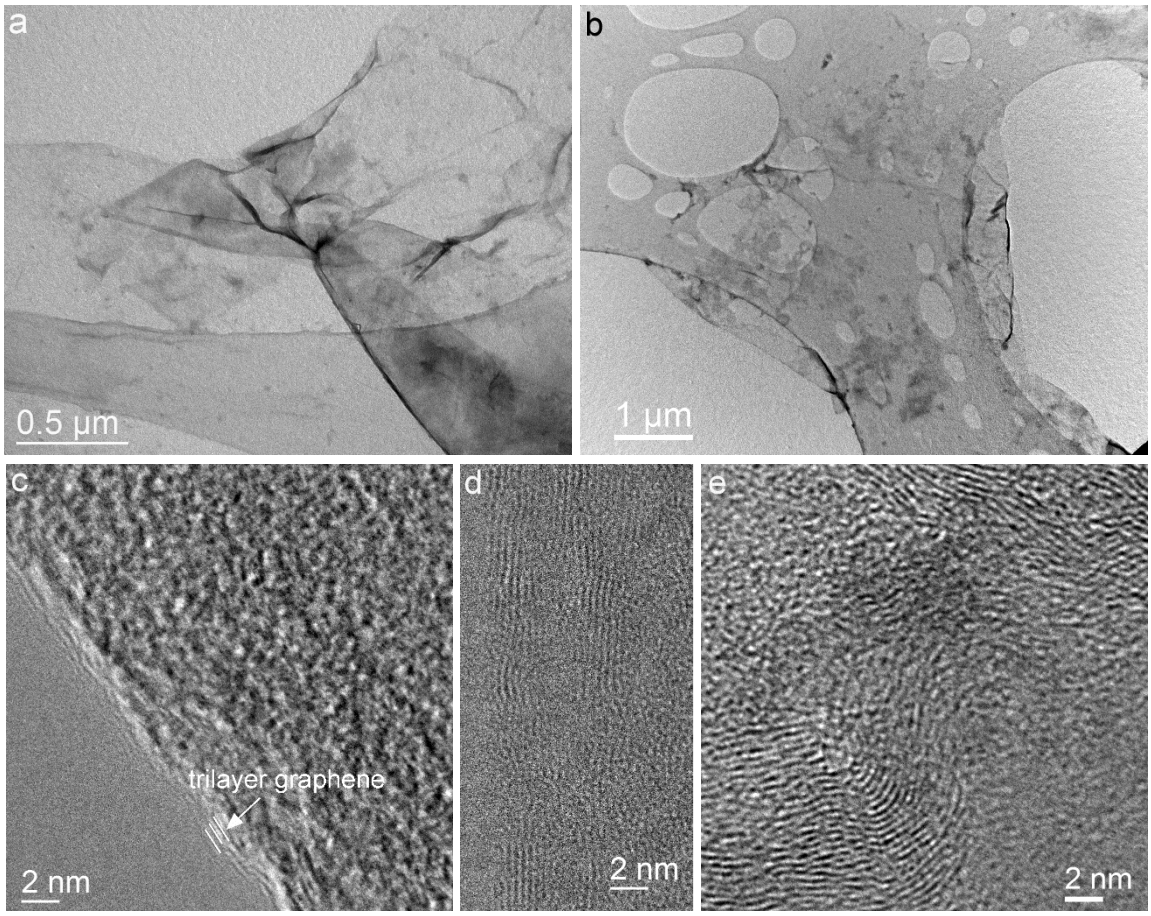

Fig. 4 TEM images of transferred free surface graphene-based carbon film synthesized at 350 °C for 12 h: (a and b) low magnification TEM image of thin graphene films with size up to several micrometers; (c) and (d) the corresponding HRTEM images of thin graphene layers of (a) and (b) showing the multilayered graphene with a thickness from 3 atomic carbon layers to 6 atomic carbon layers; (e) HRTEM images of thick graphene segments.

To disclose the graphene-based carbon film formed on free surface of Ni, we revealed its microstructure by using transmission electron microscopy. Fig. 4 shows the plane-view TEM images of transferred free surface graphene film. As shown in Fig. 4a and b, the film is thin and in large area up to several microns and continuous without any pore. The HR-TEM micrographs in Fig. 4c-e show the stacked layer structure of multilayer graphene. All the distance between parallel planes is 0.34 nm, corresponding to the (002) plane of graphitic carbon. No clear observation of amorphous carbon could be done because the amorphous carbon concentration is low and attached on the graphene surface. Fig. 4c displays trilayer

graphene corresponding to the film shown in Fig. 4a. Also multilayered graphene segments with 6 atomic carbon layers as shown in Fig. 4d were detected in the film. We also checked the dark graphene segments as shown in Fig. 2b. The thick graphene segments have ~20 layers as depicted in Fig. 4e. In conclusion, the free surface graphene-based carbon film consists of graphene segments of different thicknesses, mainly of 3~6 atomic carbon layers and a few segments of more than 10 atomic carbon layers. The HR-TEM results also illustrate that the thin graphene segments contains many defects, distorted layers, and low graphitization, therefore decreasing the graphene quality. Nevertheless, the results prove the success of synthesizing multilayer graphene segments at such a low temperature of below 350 °C. Apparently the size of graphene segments is much larger than the Ni grains, indicating the possibility of crossing grain boundary growth at rather low temperature. Additionally, the multilayered graphene segments form a continuous thin film, which could be used for transparent conductive electrodes, anti-corrosion protection layer, ion selective membranes etc.

For the sake of comparison, Fig. 5 shows the different microstructure of interface graphene grown at Ni/SiO_2 interface at 350 °C. As seen at a lower magnification in TEM (see Fig. 5a), it shows a flexible and thicker interface graphene-based carbon film, consistent with the results from optical microscope. Different areas of the interface graphene film were observed with HR-TEM. As shown in Fig. 5b, the edge area marked with a dashed box in Fig. 5a contains more than 10 atomic layers. The wrinkles marked by a white dashed circle even show ~30 layers graphene due to folding. Combining with Raman spectroscopic analysis, optical observation and TEM results, it is concluded that the interface graphene-based carbon film is thicker and contains a higher content of defects.

3.2 graphene growth on Ni surface and its growth mechanism

In order to understand the graphene growth process on Ni free surface at low such temperatures, a Ni thin film composed of less than 10 nm Ni crystals was deposited on an amorphous carbon TEM grid and underwent vacuum thermal processing at 350 °C for 12 hrs to grow graphene film (see SEM, HR-TEM and SAED pattern in Fig. S4 and S5). The amorphous carbon film grid served as carbon source. Before vacuum heat treatment, no graphene segments were observed as shown in the TEM micrographs of Fig. 6a and 6c. After vacuum thermal processing at 350 °C for 12 hrs, on the free surface of Ni there were micron-sized graphene segments formed as can be seen in Fig. 6b and the SEM image in the Supplementary Fig. S5a. Meanwhile, the grain size of Ni increased slightly but it was still smaller than 20 nm (see Supplementary Fig. S5b). Fig. 6d shows the HR-TEM image of the

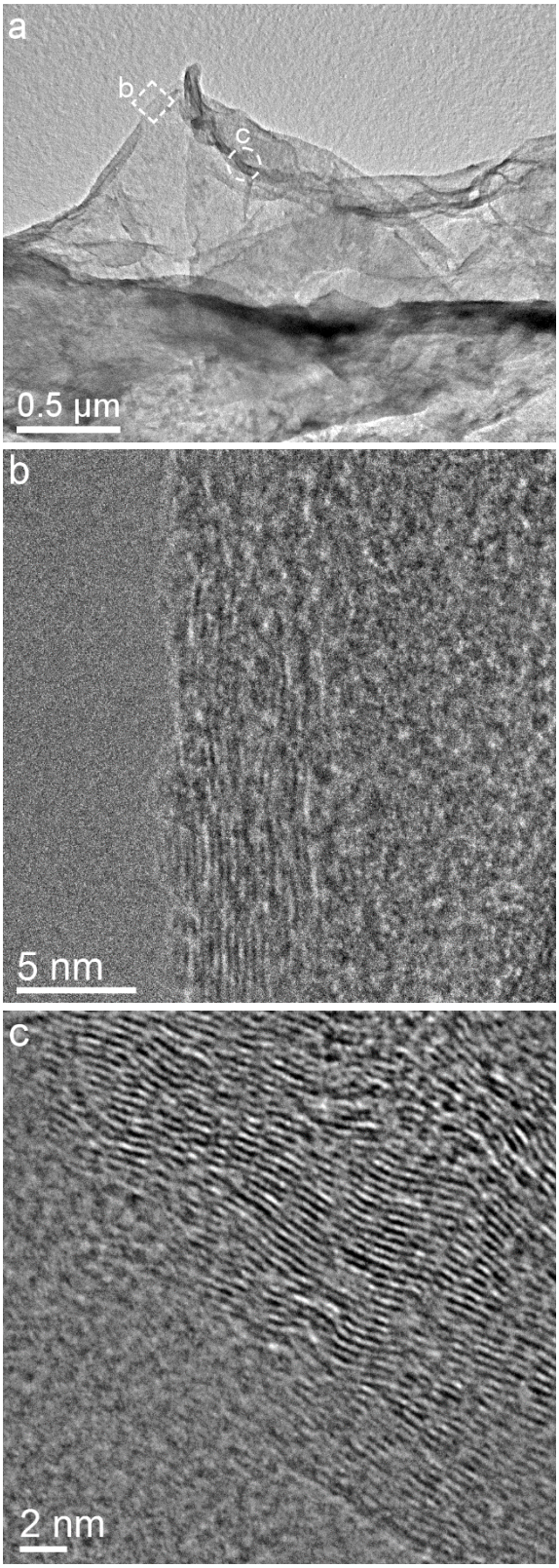

Fig. 5 TEM images of interface graphene-based carbon film grown at 350 °C for 12h: (a) low magnification image, (b) HR-TEM image of the edge marked in (a) reveals the thick layers of interface graphene, (c) HR-TEM image of the wrinkle indicated in (a).

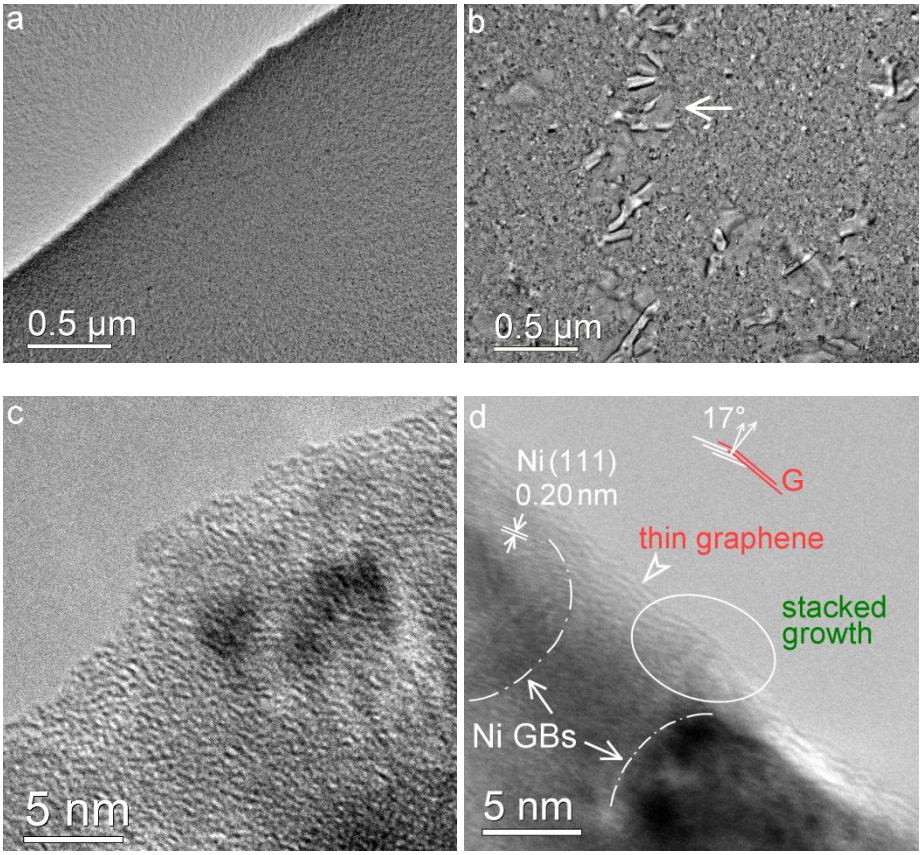

Fig. 6 (a, b) low magnification TEM micrographs of Ni thin film coated amorphous carbon grid before and after vacuum thermal treatment at 350 °C for 12h, respectively. (c-d) HRTEM of the edges of the sample before and after vacuum thermal treatment at 350 °C for 12h.

Ni-C interface, demonstrating a trilayer graphene film grown on Ni film. The graphene film has a curved surface and contains geometrically necessary dislocations that can be seen from the side view of graphene layers in Fig. 6d. It should be emphasized that the graphene segment grew on terraces, along the ledges and kinks on Ni (111), then crossed the Ni grain boundary, and form long tails away from the Ni (111) ledges and kinks. Also an angle of 17 ° between graphene (002) orientation and the Ni (111) orientation is different with previous observations that the graphene (002) orientation parallels the Ni (111) orientation. The angle may be consistent with the Ni-C interfacial ledges, analogous to the observations of CNT formation on Ni nanoparticles, proving the epitaxial growth [42].

Graphene growth is considered to be conformal to Ni catalyst grains because the Ni (111) layer is nearly atomically coherent with the basal plane of graphite [8]. It can be seen in Fig. 6d that the size of graphene sheets is much larger than the Ni grain size (≤ 20 nm), indicating the growth of graphene crossing Ni GBs. When two graphene sheets formed on different Ni (111) grains run into each other near Ni grain-boundaries, the graphene layers could become

stacked. A stacked region over the Ni grain-boundaries marked by a white ellipse is shown in Fig. 6d. The stacked growth could be the reason for generation of the mixed tilt-twist dislocations patterns as observed in Fig. 4d and Fig. 5c. Thus, the formation of graphene segments up to microns could be attributed to the synergetic effect of crossing grain boundaries growth and stacking.

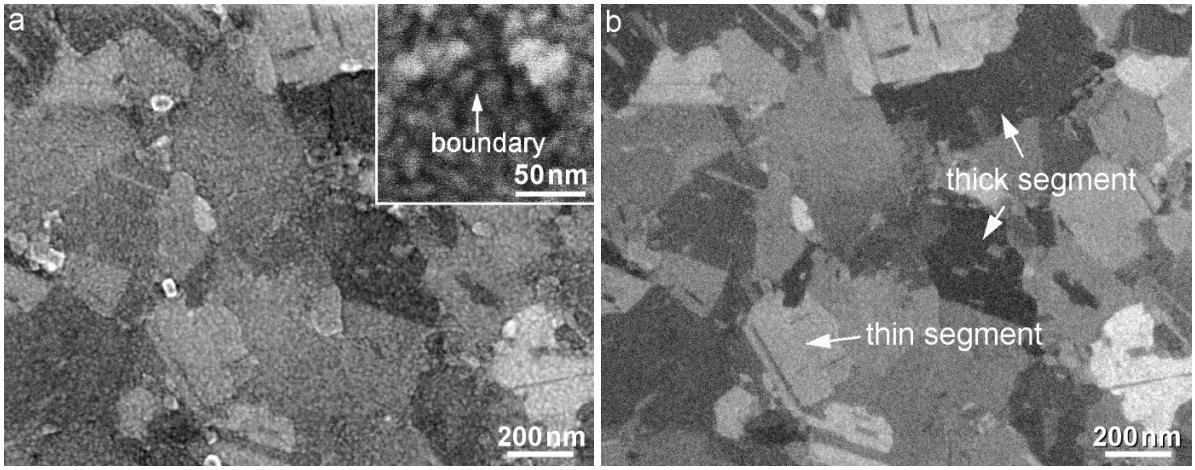

Fig. 7 High-resolution SEM images revealing the topographic contrast (a) and voltage contrast (b) of the same field of view of the graphene layer formed on the surface of Ni film to show the differentiation of graphene segments with different thicknesses. Inset of (a) shows a graphene segment crossing the Ni grain boundaries, as well as the darker boundary areas (more graphene layers).

High-resolution SEM micrographs in Fig. 7 present direct evidence of the large area growth and polycrystalline nature of the multilayered graphene film. This is demonstrated by the topographic contrast and voltage contrast of the same field of view to reveal the micrometer-sized graphene segments which have grown on the free surface and cross the grain boundary of much smaller Ni grains (< 20 nm). As a result full coverage is achieved of the entire surface of the Ni sample. As the graphene segments are conformal onto the underneath Ni film, the grainy morphology and nanometer-sized Ni grains of the underneath Ni film are well recognized in the topographic contrast SEM micrograph (Fig. 7a), together with a weak contrast showing the graphene segments of micrometer sizes and sharp edges (boundaries). In contrast, the polycrystalline structure and different thicknesses of large area multilayered graphene films are revealed in the voltage contrast micrograph of the same field of view (Fig. 7b). The grey levels are an indication of the thickness of the multilayered graphene segments. The inset in Fig. 7a highlights that a graphene segment crosses the nc-Ni grain boundaries and coats many Ni grains. By a closer inspection, we also found darker grain boundary areas, corresponding to thicker stacked graphene layers. This discloses that the boundary areas are

the places where the diffusion of carbon atoms, nucleation and growth of graphene occur quite fast. In the light of graphene stacking on the boundary area, graphene can form a large area on nc-Ni films.

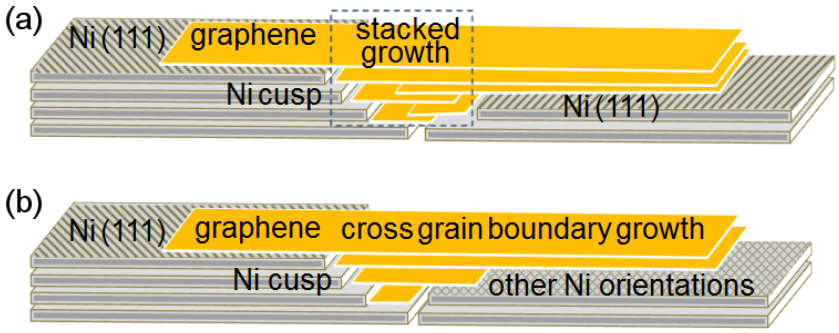

Fig. 8 Schematic illustration of the graphene growth by the diffusion and conversion of amorphous carbon: (a) stacked growth such that the elongated graphene generated from Ni (111) planes but with misorientation stacked together and then formed a whole graphene film; (b) crossing grain boundary growth that the elongated graphene generated from Ni(111) planes cross the Ni grain boundaries to other neighbor Ni planes such as (110), (100) etc.

The physical picture which emerges is schematically shown in Fig. 8. Carbon atoms diffuse through the Ni films, from the carbon reservoir, and precipitate on the Ni (111) planes. Due to the higher diffusivity of carbon along grain-boundaries than through the interior of Ni grains, the carbon atoms nucleate first at Ni grain-boundaries. The Ni (111) cusps become active sites for the Ni-C interaction and the nucleation of graphene [43]. Thereafter, graphene nuclei grow laterally mainly by the fast surface diffusion of carbon. Subsequently the graphene covers the local Ni grains. As Ni grains have different orientations in the sputter deposited thin films, the growth of graphene may have two situations: (i) stacking effect between Ni {111} grains. For the various Ni {111} textured grains, the graphene grown on both of them (Fig. 8a), and do not coincide, but stacked together at Ni grain boundaries and result in the distortion and dislocation structures as shown in Fig. 4e and Fig. 5c. (ii) crossing grain boundary growth from a Ni {111} grain onto non-{111} Ni grains. On non-{111} Ni grains, graphene exhibits different growth behavior and lower growth rate [44]. In the cusp of one grain with (111) plane and another grain with non-(111) plane, the graphene may first nucleate on the (111) cusp and propagate cross the boundaries, extend to the neighbor grain, and continuously grow on it, as shown in Fig. 8b. This could happen because of the epitaxial growth of graphene and the fast surface carbon diffusion on the catalyst surface. The formation of graphene sheets of different thicknesses may be attributed, not so much to thermodynamics equilibrium arguments, but to arguments based on kinetics, i.e. to the faster growth rate of graphene near the grain boundaries.

Thus, we consider the formation of graphene segments on nc-Ni surface is ascribed to the above two synergetic growth mechanisms. We may conclude that crossing grain boundary growth and stacking growth behaviors reflect the complex processes involved at the various stages such as feedstock dissociation, carbon diffusion, segregation on the steps, and graphene extrusion.

3.3 Dynamic growth process and influencing parameters

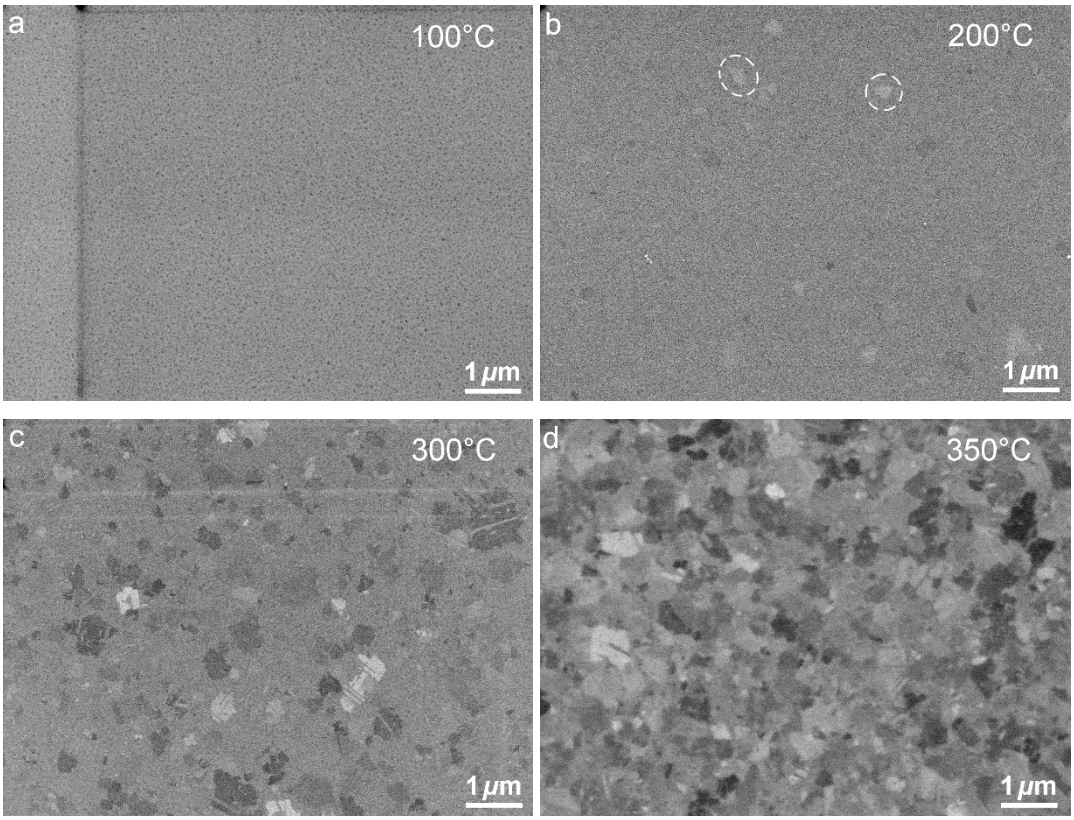

Fig. 9 SEM micrographs showing the formation of graphene segments on the free surface of the Ni-C-Ni sandwich film samples processed by VTP for 1 h at different temperatures: (a) 100 °C, (b) 200 °C, (c) 300 °C and (d) 350 °C.

The annealing temperature (*T*) of the vacuum thermal process is one of the most significant factors because it not only influences the growth kinetics of graphene but also the diffusion rate of carbon atoms in Ni films. Fig. 9 and Fig. 10 illustrate the morphology and density change of graphene segments on Ni surface when varying *T* from room temperature to 350 °C for 1 h VTP. It can be seen in Fig. 9a that small graphene segments (~20 nm) were generated but with a very low coverage (~16 %), indicating already formation of graphene at 100 °C. When *T* was 200 °C, more graphene domains were generated and formed a continuous film with a high coverage of ~98.8 %, except for a few bare Ni surface areas encircled in Fig. 9b. Also, thick

graphene segments started to form. With VTP at 300 °C, more thick graphene segments appeared and accounted for ~15.3% area fraction, and the thin graphene films was down to ~84.4 %. When *T* increased a little higher to 350 °C, much more thick graphene segments were generated and reached a higher coverage of ~48%, while the coverage of the thin graphene decreased to ~51%. This observation clearly reveals that vacuum thermal processing at higher temperatures leads to the growth of graphene from small domains to large segments, and from thin graphene film to thick graphene sheets. Especially when *T* is above 300 °C, temperature becomes a more sensitive parameter on the formation of thick graphene segments (see Fig. 10). Actually, even at room temperature the carbon atoms are mobile and nucleate in the form of graphitic structure as shown in Fig. S5 [25]. For example, after keeping the Ni film coated C grid for 2 weeks at room temperature without any vacuum thermal processing treatment, some lattice fringes indexed to the (002) of graphitic crystals were observed as shown in Fig. S7.

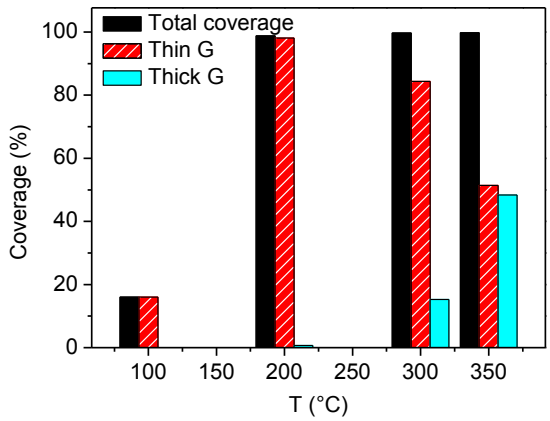

Fig. 10 The coverage of graphene segments on the sandwich samples VTP treated for 1 h at different temperatures from 100 to 350 °C (Thin G: thin graphene film, Thick G: thick graphene segments).

The processing time is another important factor for graphene growth at low temperatures. We investigated the treatment time from 1 min to 96 hrs to examine the growth kinetics of the free surface graphene film on Ni, as shown in Fig. 11 and 12. It was found that within 1 min, graphene has already grown to a coverage of 97.2%, and thick graphene segments started to form (~7.1% of coverage, see Fig. 12). Fast graphene formation reveals a high diffusivity of carbon atoms and growth of graphene. With vacuum thermal processing for 10 min, more thick graphene segments formed (~12.9% as shown in Fig. 12), and the graphene cover almost the entire surface (~98.1%). With increasing *t* to 1 h, the fraction of thick graphene segments was substantially increased to 48.0% and thin graphene films decreased to 51.5%. Up to 96 hrs annealing, it can be seen that larger and thicker graphene segments become dominant with a

fraction of ~80.2%. Extending the VTP time from 1 min to 96 hrs, in addition to the increase in the thickness and coverage of graphene film, also the individual graphene segments extended (see Fig. 11b and 11d). From these observations, it should be emphasized that the growth rate of thin graphene films is much faster than the growth of thick graphene segments indicating a complicated carbon diffusion and reaction processes.

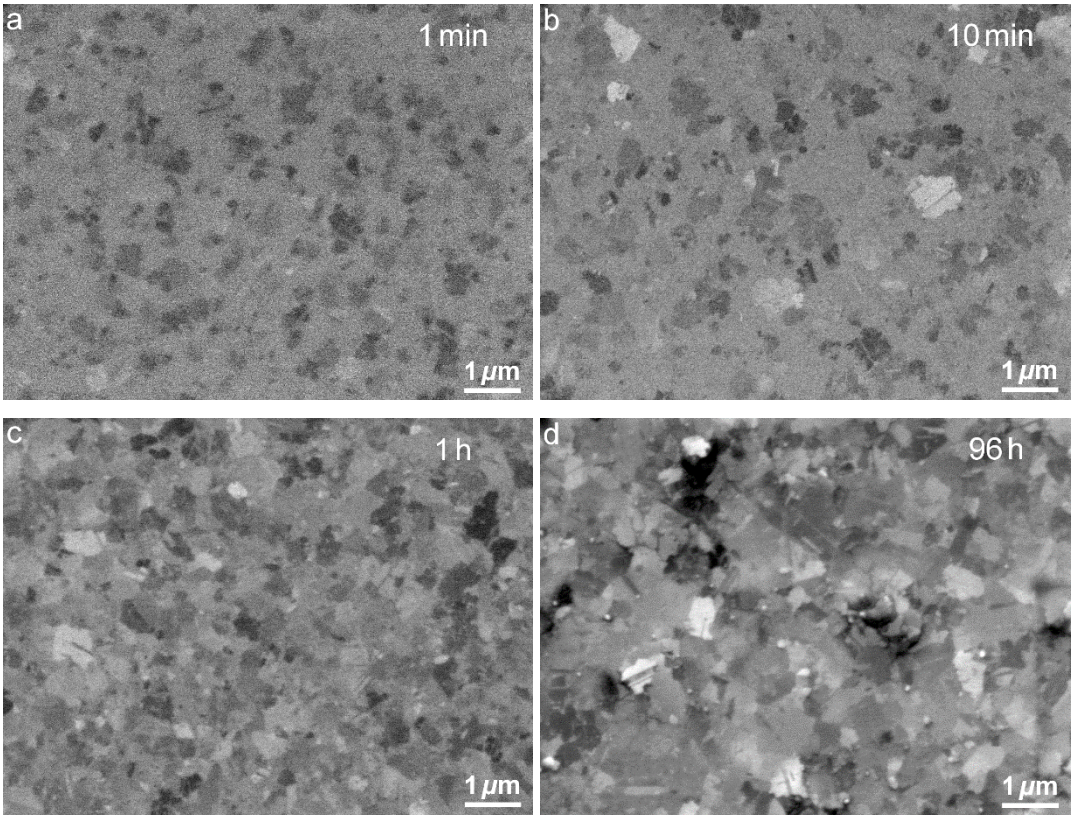

Fig. 11 SEM images of the surfaces of the Ni-C-Ni sandwich film prepared by VTP at 350 °C for different times: (a) 1 min, (b) 10 min, (c) 1 h and (d) 96 h.

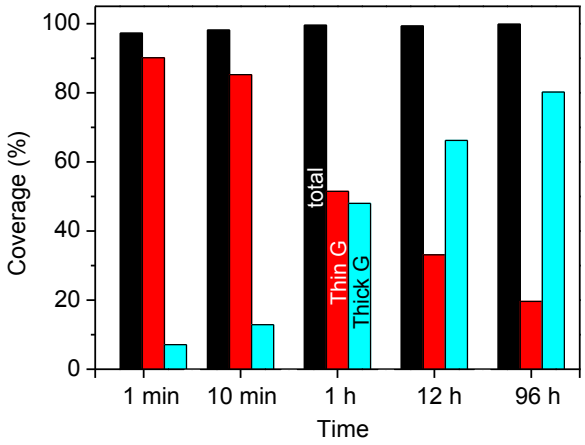

Fig. 12 The coverage of graphene films prepared at 350 °C for various time: from 1 min to 96 h (Thin G: thin graphene, Thick G: thick graphene segments).

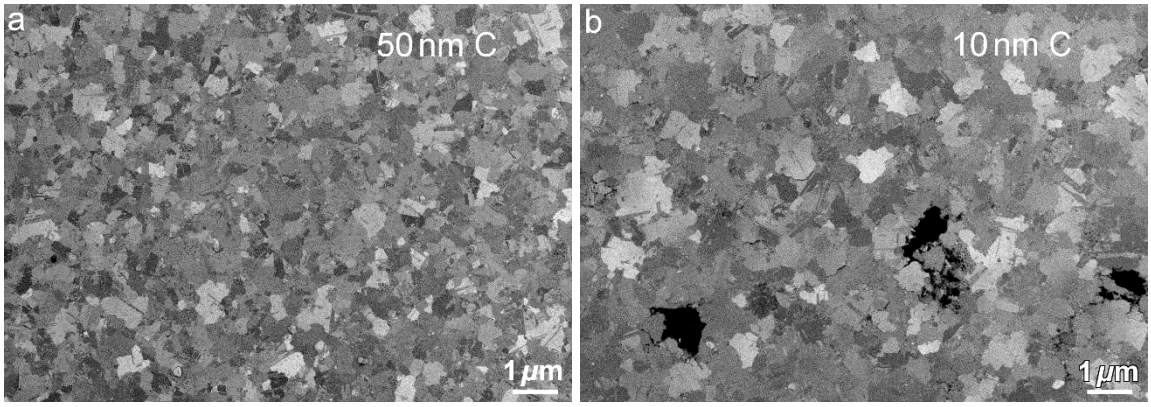

Fig. 13 SEM images revealing the graphene layer formed after VTP at 350°C for 96 h on the surface of Ni-C-Ni sandwich film composed of (a) 50 nm thick carbon film and (b) 10 nm thick carbon film.

In this work, amorphous carbon was used as a feedstock. The reason is that most of gaseous carbon resources require a high decomposition temperature. The fast carbon diffusivity through Ni film and low temperature coating technique make amorphous carbon being an adequate resource. We decreased the thickness of carbon films from 100 nm to 50 nm, and further to 10 nm (namely changing Ni to C film thickness ratio from 2:1 down to 4:1 and 20:1, coded as Ni-C(2:1), Ni-C(4:1), and Ni-C(20:1), respectively) for scrutinizing the effect of source carbon content on the formation of graphene. To make sure that the carbon films exhausted as much as possible, vacuum thermal processing was performed at 350 °C for 96 hrs. Comparing with Ni-C(2:1) shown in Fig. 11d, the sample Ni-C(4:1) does not show obvious difference as seen in Fig. 13a, but the sample Ni-C(20:1) demonstrates smaller coverage ~92.3%, less thick graphene segments formed with a coverage fraction of 14.5%, and more uniform films (see Fig. 13b). Importantly, we found most of the graphene domains of sample Ni-C(20:1) is thinner and larger than those of Ni-C(2:1) and Ni-C(4:1). These two different characteristics revealed a smaller diffusion flux of carbon under limited carbon content and less graphene domains nucleated. We checked the remaining carbon film after VTP, and found that less than 10% of carbon was consumed in sample Ni-C(2:1) (see Fig. S8a). In contrast, the carbon film was fully exhausted in sample Ni-C(20:1) (see Fig. S9a). In theory, the carbon diffusion flux through Ni can be largely influenced by the carbon concentration under non-steady state diffusion due to limited carbon source. Diffusion flux of carbon gets smaller and causes low carbon concentration onto the Ni surface in the graphene induction period, leading to less graphene nuclei and slower growth. Less graphene nucleation helps generate larger graphene segments. The thinner graphene was thus formed due to the less provided carbon. Therefore, adjusting

the carbon/Ni ratio is a good strategy for controlling the graphene thickness, domain size and coverage, ever for controlling monolayer graphene growth.

A point of discussion is the diffusional processes and time scale involved. To form thin or thick graphene films on Ni surface and along Ni/SiO_2 interface diffusional processes of C are required. Bulk diffusion of carbon through an interstitial mechanism in pure nickel is rather difficult and requires 1.7 eV/atom (163.9 kJ/mol) from octahedral site via tetrahedral sites to another octahedral site. In the current situation the structures of nanometer sized Ni grains are helpful and promote grain-boundary diffusion to the outer Ni free surface. The activation energy for grain-boundary diffusion is usually 1/3-1/2 of the bulk diffusion value (0.57-0.85 eV).

Taking the experimental value of the pre-factor in the Boltzmann description of the diffusional process of C in Ni equal to $D_0 = 2\times10^{-9}$ $m^2 \cdot s^{-1}$ [25], leads to the conclusion that at 350 °C it only takes of the order of seconds to cross a distance of 100 nm from the amorphous C to the free surface of Ni (see Fig. 1) through grain boundary diffusion. Surface diffusion on a {111} planes of Ni is even faster because of an even lower activation energy of 45 kJ/mol (0.47 eV/atom). To give an idea in numbers: a surface area of Ni with the size of 10×10 μm² can be covered in 3 minutes with carbon at 350 °C as having been confirmed by our experimental findings.

Interestingly, theoretical calculations based on density functional theory and experiments suggest that sub-surface diffusion of C along a {111} plane occurs at a fairly high rate, i.e. close to grain-boundary diffusion with an activation energy of 0.9 eV [45,46]. In fact, if C is present in a sub-surface layer, the most favorable process for carbon diffusion is to move laterally, i.e. perpendicular to the <111> surface normal of the free surface along the {111} plane in Ni, making use of the octahedral-tetrahedral-octahedral pathway. This lateral process is promoted because diffusion towards the bulk needs much higher activation energy (say above 1.7 eV) but also backward diffusion to the free surface is less likely (activation energy 1.16 eV). Indeed carbon in an octahedral site creates also lateral straining (around 9% at the surface) and to make a patch of graphene needs quite a bit of mechanical energy which is not very likely to occur. Other systems including ordered structures and compounds may cope with this problem and will assist the formation of even sub-surface graphene layers which is an interesting idea to explore making the method even more facile.

4. Conclusions

The ultimate objective of this study is to synthesize large-area graphene-based carbon films through a new approach to present a fast and low temperature method. It is concluded that micrometer-sized graphene segments can be synthesized to a full coverage of a Ni surface using low temperature (< 350 °C) thermal vacuum processing and conversion of amorphous carbon. It is confirmed through electron microscopy that thin graphene segments (3-6 layers) and thick graphene segments (more than 10 layers) are grown on the Ni free surface. Growth parameters such as growth time, growth temperature and C/Ni ratio are investigated in detail for the kinetic control of graphene growth.

An important conclusion is that the complete coverage of Ni surface by graphene-based carbon can be achieved within a time as short as 1 minute. An overall conclusion and outlook is that this work provides a competitive strategy for manufacturing of graphene-based carbon coated surfaces at an industrial scale and that the quality of as-grown graphene-based carbon films can be further enhanced.

Acknowledgements

The authors gratefully acknowledge the financial support from the Faculty of Science and Engineering, University of Groningen, The Netherlands. We sincerely thank Professor Wesley R. Browne for valuable discussion and support to the Raman analysis of graphene samples. Dr. Roland Schmidt at Hitachi High-Technologies Europe GmbH, Krefeld, Germany, is thanked for high resolution SEM observation of graphene layers with Hitachi SU8230.

Reference

[1] A.H. Castro Neto, F. Guinea, N.M.R. Peres, K.S. Novoselov, A.K. Geim, The electronic properties of graphene, Rev. Mod. Phys. 81 (2009) 109.

[2] F. Bonaccorso, L. Colombo, G. Yu, M. Stoller, V. Tozzini, A.C. Ferrari, et al., Graphene, related two-dimensional crystals, and hybrid systems for energy conversion and storage, Science 347 (2015) 1246501-1.

[3] T. Lin, I.W. Chen, F. Liu, C. Yang, H. Bi, F. Xu, et al., Nitrogen-doped mesoporous carbon of extraordinary capacitance for electrochemical energy storage, Science 350 (2015) 1508-1513.

[4] C. Chung, Y.K. Kim, D. Shin, S.R. Ryoo, B.H. Hong, D.H. Min, Biomedical applications of graphene and graphene oxide, Acc. Chem. Res. 46 (2013) 2211-2224.

[5] X.K. Kong, C.L. Chen, Q.W. Chen, Doped graphene for metal-free catalysis, Chem. Soc. Rev. 43 (2014) 2841-2857.

[6] V. Chabot, D. Higgins, A. Yu, X. Xiao, Z. Chen, J. Zhang, A review of graphene and graphene oxide sponge: material synthesis and applications to energy and the environment, Energy Environ. Sci. 7 (2014) 1564-1596.

[7] M. Fathizadeh, W. L. Xu, F.L. Zhou, Y. Yoon, M. Yu , Graphene Oxide: A Novel 2-Dimensional Material in Membrane Separation for Water Purification, Adv. Mater. Interfaces 4 (2017) 1600918.

[8] Z. Yan, Z. Peng, J.M. Tour, Chemical vapor deposition of graphene single crystals, Acc. Chem. Res. 47 (2014) 1327-1337.

[9] M. Zhou, T. Lin, F. Huang, Y. Zhong, Z. Wang, Y. Tang, et al., Highly conductive porous graphene/ceramic composites for heat transfer and thermal energy storage, Adv. Funct. Mater. 23 (2013) 2263-2269.

[10] I. A. Kostogrud , K. V. Trusov , D. V. Smovzh, Influence of Gas Mixture and Temperature on AP-CVD Synthesis of Graphene on Copper Foil, Adv. Mater. Interfaces 3 (2016) 1500823.

[11] Z. Sun, Z. Yan, J. Yao, E. Beitler, Y. Zhu, J. M. Tour, Growth of graphene from solid carbon sources, Nature 468 (2010) 549-552.

[12] W. Xiong, Y.S. Zhou, L.J. Jiang, A. Sarkar, M. Mahjouri-Samani, Z.Q. Xie, et al., Single-step formation of graphene on dielectric surfaces, Adv. Mater. 25 (2013) 630-634.

[13] Z. Li, P. Wu, C. Wang, X. Fan, W. Zhang, X. Zhai, et al., Low-temperature growth of graphene by chemical vapor deposition using solid and liquid carbon sources, ACS Nano 5 (2011) 3385-3390.

[14] J. Zhang, J. Li, Z. Wang, X. Wang, W. Feng, W. Zheng, et al., Low-temperature growth of large-area heteroatom-doped graphene film, Chem. Mater. 26 (2014) 2460-2466.

[15] B. Zhang, W.H. Lee, R. Piner, I. Kholmanov, Y. Wu, H. Li, et al., Low-temperature chemical vapor deposition growth of graphene from toluene on electropolished copper foils, ACS Nano 6 (2012) 2471–2476.

[16] M. Zhu, Z. Du, Z. Yin, W. Zhou, Z. Liu, S. H. Tsang, et al., Low-temperature in situ growth of graphene on metallic substrates and its application in anticorrosion, ACS Appl. Mater. Interfaces 8 (2016) 502-510.

[17] R.S. Weatherup, B.C. Bayer, R. Blume, C. Ducati, C. Baehtz, R. Schlögl, et al., In situ characterization of alloy catalysts for low-temperature graphene growth, Nano Lett. 11 (2011) 4154-4160.

[18] J. Kim, M. Ishihara, Y. Koga, K. Tsugawa, M. Hasegawa, S. Iijima, Low-temperature synthesis of graphene on nickel foil by microwave plasma chemical vapor deposition, Appl. Phys. Lett. 98 (2011) 263106.

[19] C.S. Lee, C.S. Cojocaru, W. Moujahid, B. Lebental, M. Chaigneau, M. Châtelet, et al., Synthesis of conducting transparent few-layer graphene directly on glass at 450 °C, Nanotechnology 23 (2012) 265603.

[20] G. Gutierrez, F. Le Normand, D. Muller, F. Aweke, C. Speisser, F. Antoni, et al., Multi-layer graphene obtained by high temperature carbon implantation into nickel films, Carbon 66 (2014) 1-10.

[21] R. Vishwakarma, M.S. Rosmi, K. Takahashi, Y. Wakamatsu, Y. Yaakob, M. I. Araby, et al., Transfer free graphene growth on SiO_2 substrate at 250 °C, Sci. Rep. 7 (2017) 43756.

[22] M.H. Rümmeli, A. Bachmatiuk, A. Scott, F. Börrnert, J.H. Warner, V. Hoffman, et al., Direct low-temperature nanographene CVD synthesis over a dielectric insulator, ACS Nano 4 (2010) 4206-4210.

[23] A. Scott, A. Dianat, F. Börrnert, A. Bachmatiuk, S. Zhang, J. H. Warner, et al., The catalytic potential of high-κ dielectrics for graphene formation, Appl. Phys. Lett. 98 (2011) 073110.

[24] Y. Gamo, A. Nagashima, M. Wakabayashi, M. Terai, C. Oshima, Atomic structure of monolayer graphite formed on Ni(111), Surf. Sci. 374 (1997) 61-64.

[25] J. Kwak, J.H. Chu, J. Choi, S.D. Park, H. Go, S.Y. Kim, et al., Near room-temperature synthesis of transfer-free graphene films, Nat. Commun. 3 (2012) 645.

[26] E.V. Zhizhin, D.A. Pudikov, A.G. Rybkin, A.E. Petukhov, Y.M. Zhukov, A.M. Shikin, Growth of graphene monolayer by "internal solid-state carbon source": Electronic structure, morphology and Au intercalation, Mater. Des. 104 (2016) 284–291.

[27] M. Zheng, K. Takei, B. Hsia, H. Fang, X.B. Zhang, N. Ferralis, et al., Metal-catalyzed crystallization of amorphous carbon to graphene, Appl. Phys. Lett. 96 (2010) 063110.

[28] C.H. Zhang, S.L. Zhao, C.H. Jin, A.L. Koh, Y. Zhou, W.G. Xu, et al., Direct growth of large-area graphene and boron nitride heterostructures by a co-segregation method, Nat. Commun. 6 (2015) 6519.

[29] Y.Z. Chen, H. Medina, H.C. Lin, H.W. Tsai, T.Y. Su, Y.L. Chueh, Large-scale and patternable graphene: direct transformation of amorphous carbon film into graphene/graphite on insulators via Cu mediation engineering and its application to all-carbon based devices, Nanoscale 7 (2015) 1678.

[30] A. Barreiro, F. Borrnert, S.M. Avdoshenko, B. Rellinghaus, G. Cuniberti, M.H. Rümmeli, et al., Understanding the catalyst-free transformation of amorphous carbon into graphene by current-induced annealing, Sci. Rep. 3 (2013) 1115.

[31] U. Narula, C.M. Tan , C.S. Lai, Copper induced synthesis of graphene using amorphous carbon, Microelectron Reliab. 61 (2016) 87–90.

[32] A. Bachmatiuk, J. Boeckl, H. Smith, I. Ibrahim, T. Gemming, S. Oswald, et al., Vertical Graphene Growth from Amorphous Carbon Films Using Oxidizing Gases, J. Phys. Chem. C 119 (2015) 17965−17970.

[33] V. Kochat, A.N. Pal, E.S. Sneha, A. Sampathkumar, A. Gairola, S.A. Shivashankar, et al., High contrast imaging and thickness determination of graphene with in-column secondary electron microscopy, J. Appl. Phys. 110 (2011) 014315.

[34] A. C. Ferrari, J.C. Meyer, V. Scardaci, C.Casiraghi, M. Lazzeri, F. Mauri, et al., Raman spectrum of graphene and graphene layers, Phys. Rev. Lett. 97 (2006) 187401.

[35] A. C. Ferrari, J. Robertson, Interpretation of Raman spectra of disordered and amorphous carbon, Phys. Rev. B 61 (2000) 14095.

[36] A.C. Ferrari, D.M. Basko, Raman spectroscopy as a versatile tool for studying the properties of graphene, Nat. Nanotech. 8 (2013) 235–246.

[37] S. Claramunt, A. Varea, D. López-Díaz, M. Mercedes Velázquez, A. Cornet, A. Cirera, The importance of interbands on the interpretation of the Raman spectrum of graphene oxide, J. Phys. Chem. C 119 (2015) 10123-10129.

[38] A. Sadezky, H. Muckenhuber, H. Grothe, R. Niessner, U. Pöschl, Raman microspectroscopy of soot and related carbonaceous materials: Spectral analysis and structural information, Carbon 43 (2005) 1731–1742.

39 S. Vollebregt, R. Ishihara, F.D. Tichelaar, Y. Hou, C.I.M. Beenakker, Influence of the growth temperature on the first and secondorder Raman band ratios and widths of carbon nanotubes and fibers, Carbon 50 (2012) 3542−3554.

40 X.L. Zhao; Y. Ando, Raman spectra and X-ray diffraction patterns of carbon nanotubes prepared by hydrogen arc discharge, Jpn. J. Appl. Phys. 37 (1998) 4846-4849.

[41] E.H. M. Ferreira, M.V.O. Moutinho, F. Stavale, M.M. Lucchese, R.B. Capaz, C.A. Achete, A. Jorio, Evolution of the Raman spectra from single-, few-, and many-layer graphene with increasing disorder, Phys. Rew. B 82 (2010), 125429.

[42] S. Hofmann , R. Sharma , C. Ducati , G. Du , C. Mattevi , C. Cepek , et al., In situ observations of catalyst dynamics during surface-bound carbon nanotube nucleation, Nano Lett. 7 (2007) 602-608.

[43] J.F. Gao, J. Yip, J. Zhao, B.I. Yakobson, F. Ding, Graphene nucleation on transition metal surface: structure transformation and role of the metal step edge, J. Am. Chem. Soc. 133 (2011) 5009-5015.

[44] J. Kozlova, A. Niilisk, H. Alles, V. Sammelselg, Discontinuity and misorientation of graphene grown on nickel foil: Effect of the substrate crystallographic orientation, Carbon 94 (2015) 160-173.

[45] A. Wiltner, Ch. Linsmeier, Thermally induced reaction and diffusion of carbon films on Ni(111) and Ni(100), Surf. Sci. 602 (2008) 3623-3631.

[46] F. Cinquini, F. Delbecq, P. Sautet, A DFT comparative study of carbon adsorption and diffusion on the surface and subsurface of Ni and Ni_3Pd alloy, Phys. Chem. Chem. Phys. 11 (2009) 11546-11556.

Supplementary materials

Low-temperature synthesis of large-area graphene-based carbon films on Ni

Liqiang Lu[1], Jeff T.M. De Hosson[2], Yutao Pei[1*]

[1] *Department of Advanced Production Engineering, Engineering and Technology Institute Groningen, Faculty of Science and Engineering, University of Groningen, Nijenborgh 4, 9747 AG Groningen, The Netherlands*

[2] *Department of Applied Physics, Zernike Institute for Advanced Materials, Faculty of Science and Engineering, University of Groningen, Nijenborgh 4, 9747AG Groningen, The Netherlands*

Fig. S1a is an SEM image of the Ni-C-Ni sandwich film deposited on SiO_2 (300 nm thick)/Si substrate (500 μm thick). The size of the Ni particle is less than 20 nm. The XRD pattern shown in Fig. 1b demonstrates (111) and (200) peaks of Ni. It indicates a nanocrystalline Ni film from the large full width at half maximum (FWHM). The surface roughness was measured by using AFM. Fig. S2 is the AFM image of Ni-C-Ni sandwich film before VTP treatment. It reveals the deposited poly-Ni has a smooth surface with an RMS toughness of ~0.1 nm.

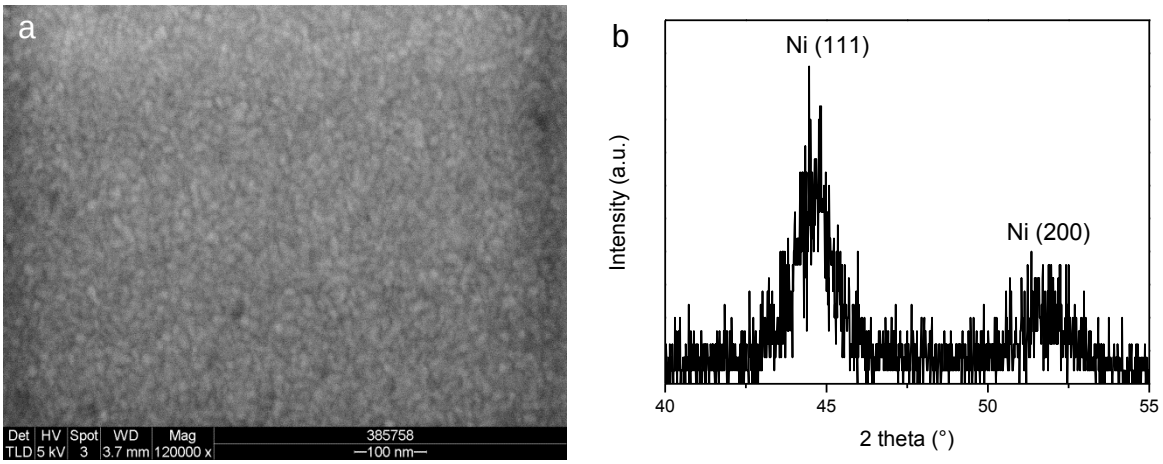

Fig. S1 SEM image (a) and XRD pattern (b) of the Ni-C-Ni sandwich film deposited on SiO_2 (300 nm thick)/Si substrate (500 μm thick).

* Corresponding author. E-mail: y.pei@rug.nl

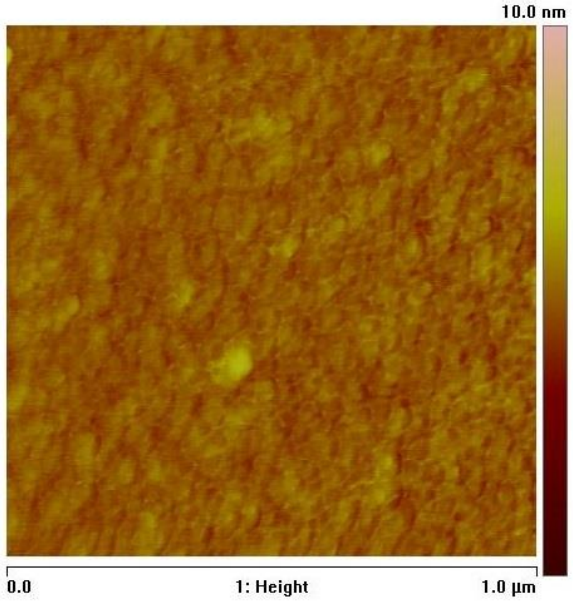

Fig. S2 AFM image of Ni-C-Ni sandwich film before annealing

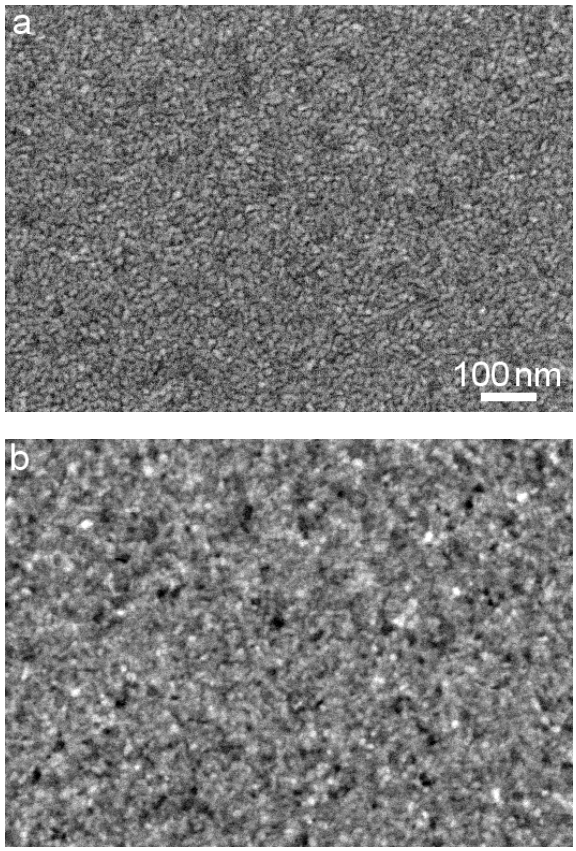

Fig. S3 High-resolution SEM images revealing the topographic contrast (a) and voltage contrast (b) of the same view field of pure nanocrystalline Ni film after VTP treatment at 350 °C for 1 h.

Table S1 Raman intensity ratio I_D/I_G and FWHM (W) of the D and G bands for the free-surface graphene and interface graphene, respectively.

	I_D/I_G	W_D (cm^{-1})	W_G (cm^{-1})
Free-surface graphene film	1.8	141	65
Interface graphene film	2.8	240	79

The calculation of I_D/I_G refers to the peak intensity of D and G peaks after deconvolution of Raman spectra as shown in Fig. 3b and Fig. 3d. The full width at half-maximum (FWHM) of the D and G peaks is listed in Table S1. The larger FWHMs for the interface graphene film indicate that the interface graphene film has a higher content of defects and smaller distances between the defects (L_D) than the free surface graphene film. The I_D/I_G of free surface graphene is also smaller than the I_D/I_G of the interface graphene, indicating a slightly better quality.

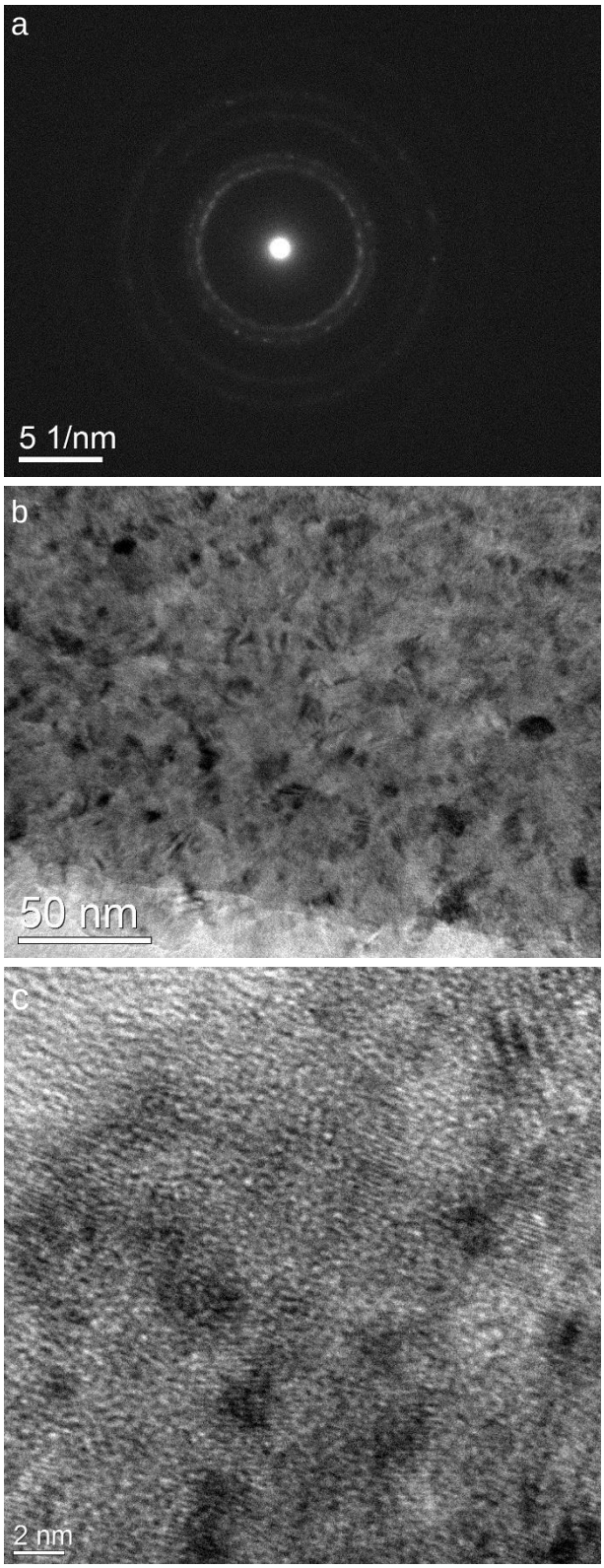

Fig. S4 SAED, TEM and HRTEM images of nc-Ni film coated amorphous carbon on Cu grids.

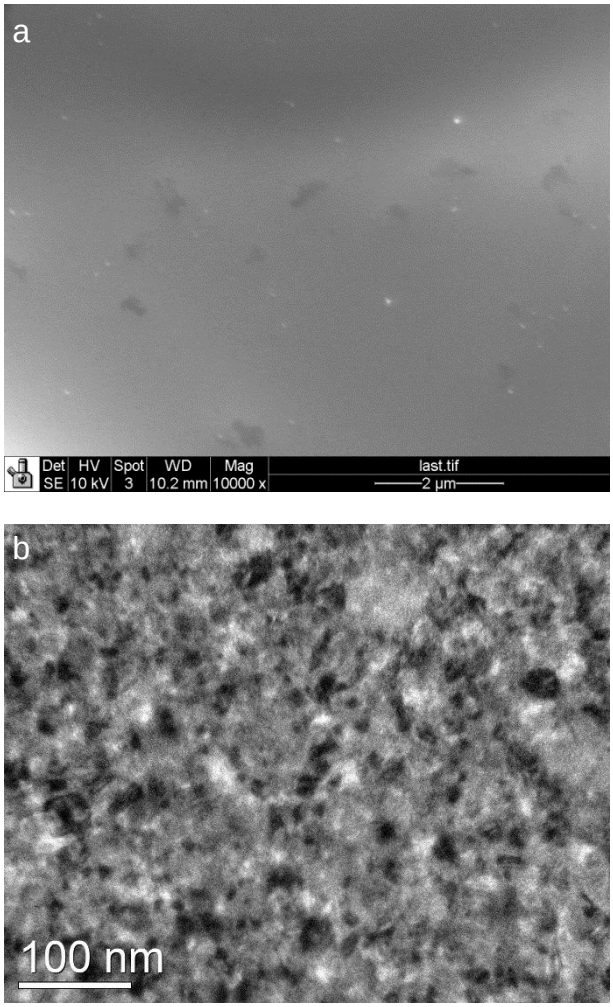

Fig. S5 (a) SEM and (b) TEM images of nc-Ni film coated amorphous carbon on Cu grid after VTP at 350 °C for 12 h.

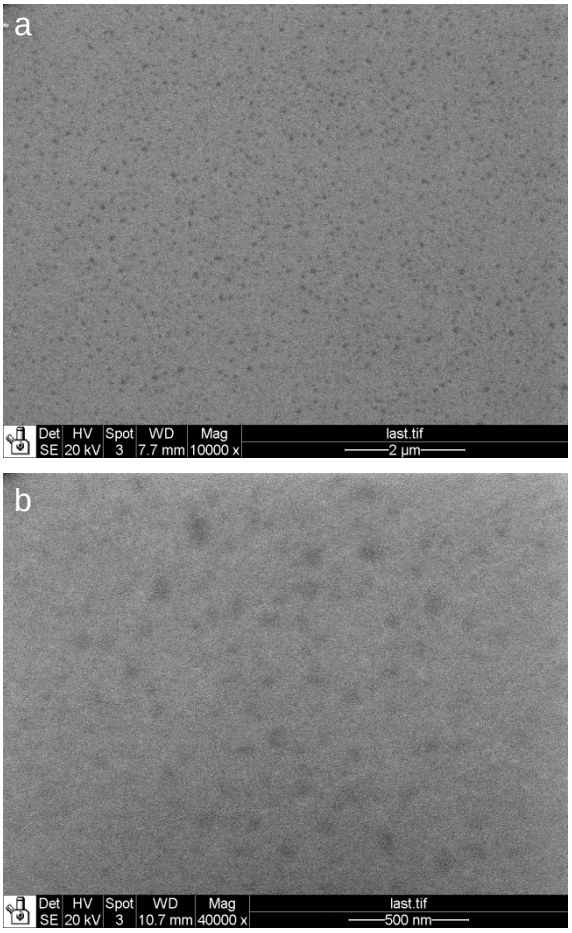

Fig. S6 SEM images of the Ni-C-Ni sandwich film kept for 4 weeks at room temperature (~20 °C). Small graphene domains start to nucleate even at room temperature, although it took a long time. This observation is consistent with the previous results of Ref. [1].

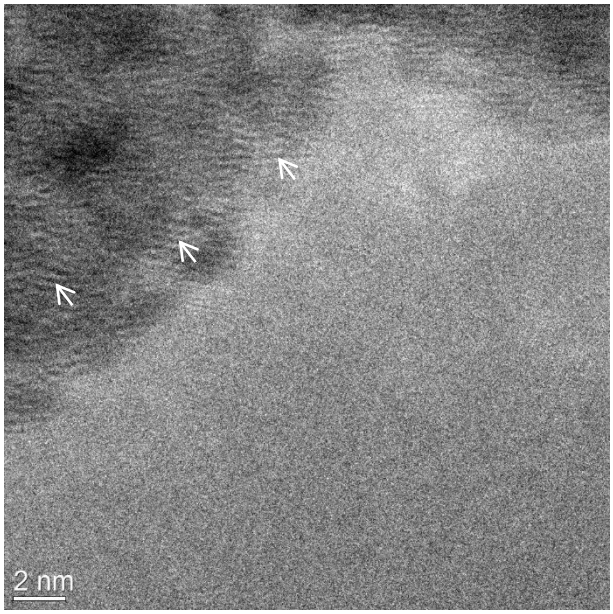

Fig. S7 HRTEM image of nc-Ni film coated amorphous carbon TEM grid kept for 2 weeks at room temperature. The white arrows show the lattice spacing of ~0.34 nm indicating graphene crystals formed at room temperature.

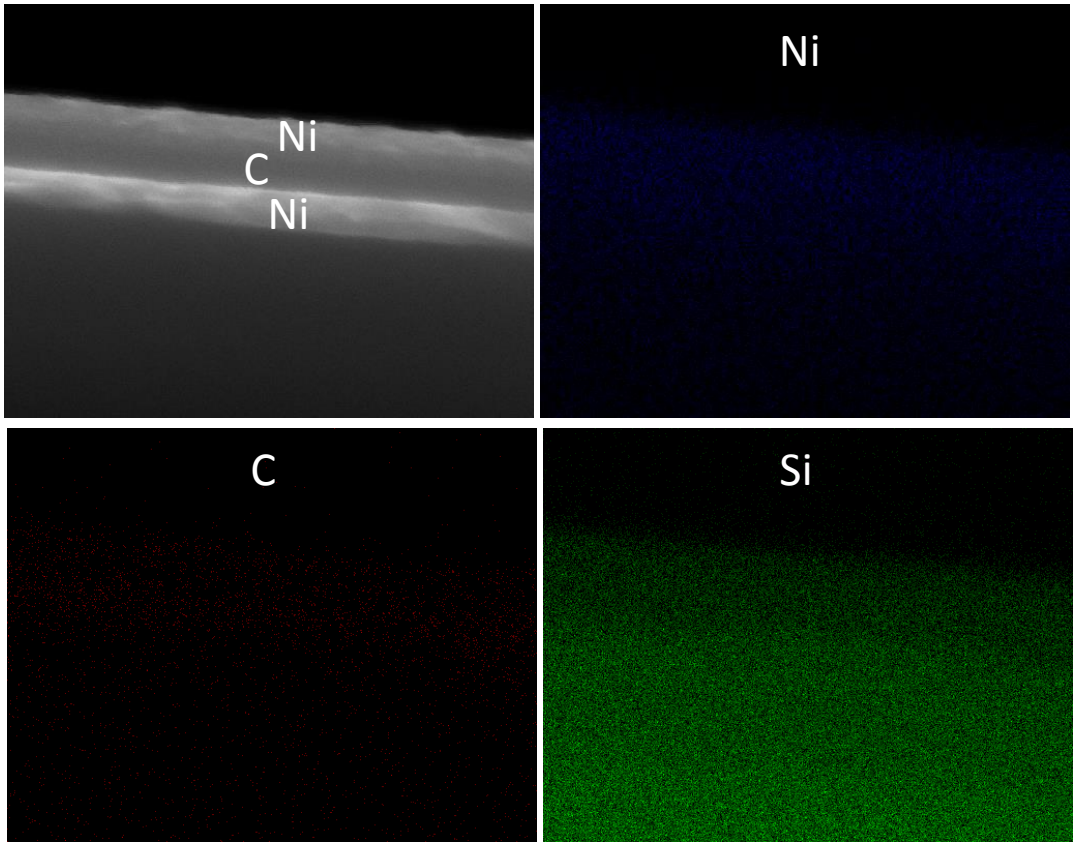

Fig. S8 Cross-sectional SEM image and element distribution of the Ni-C-Ni sandwich film with 100 nm thick carbon film after processed by VTP at 350 °C for 96 h. After VTP, abundant C still exists, indicating the Ni is saturated with C. In this case, the graphene growth mainly relies on the reaction rate instead of on reactants transport rate.

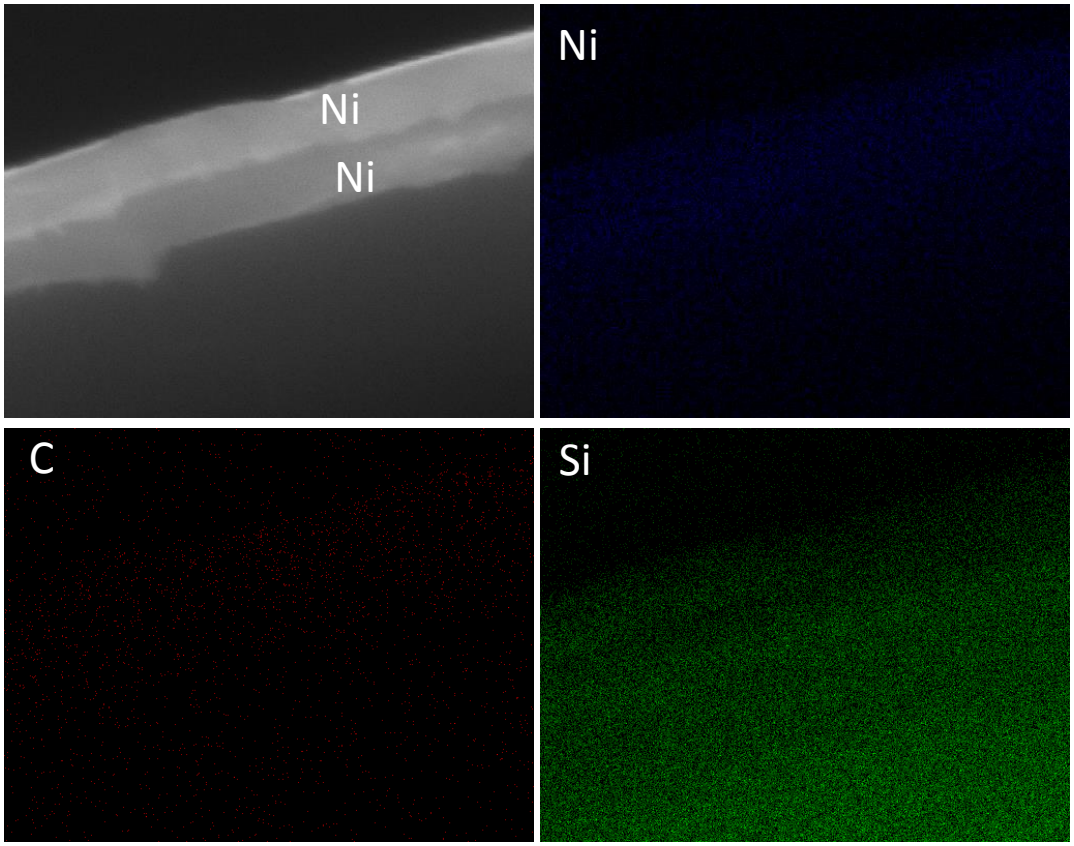

Fig. S9 Cross-sectional SEM image and element different distribution of the Ni-C-Ni sandwich film with 10 nm thick carbon film after processed by VTP at 350 °C for 96 h. After VTP, all the C film was exhausted because the carbon middle layer disappeared.

Reference:

[1] J. Kwak, J. H. Chu, J. Choi, S.D. Park, H. Go, S. Y. Kim, K. Park, S. D. Kim, Y. W. Kim, E. Yoon, S. Kodambaka, S.Y. Kwon, Near room-temperature synthesis of transfer-free graphene films, Nature Communications 3, (2012), 645.